

The Zel'dovich effect and evolution of atomic Rydberg spectra along the Periodic Table

Eugene B. Kolomeisky and Michael Timmins

*Department of Physics, University of Virginia, 382 McCormick Rd.,
P. O. Box 400714, Charlottesville, VA 22904-4714*

In 1959 Ya. B. Zel'dovich predicted that the bound-state spectrum of the non-relativistic Coulomb problem distorted at small distances by a short-range potential undergoes a peculiar reconstruction whenever this potential alone supports a low-energy scattering resonance. However documented experimental evidence of this effect has been lacking. Previous theoretical studies of this phenomenon were confined to the regime where the range of the short-ranged potential is much smaller than Bohr's radius of the Coulomb field. We go beyond this limitation by restricting ourselves to highly-excited s states. This allows us to demonstrate that along the Periodic Table of elements the Zel'dovich effect manifests itself as systematic periodic variation of the Rydberg spectra with a period proportional to the cubic root of the atomic number. This dependence, which is supported by analysis of experimental and numerical data, has its origin in the binding properties of the ionic core of the atom.

PACS numbers: 03.65.-w, 32.30.-r, 31.15.-p, 71.35.-y.

I. INTRODUCTION

In a variety of applications in physics it is important to understand how is the normal Hydrogen spectrum modified if at small distances the Coulomb law is replaced by a central short-ranged potential. An important aspect of this problem is the existence of two length scales - the Bohr radius of the Coulomb field a_B and the range of action of short-range forces r_0 .

For example, in hadronic atoms formed by charged particles and antiparticles the large distance Coulomb attraction gives its way at short distances to nuclear forces whose range r_0 is significantly smaller than a_B [1].

In condensed matter physics a similar problem is that of the energy spectrum of the Wannier-Mott exciton [2]. When in a semiconductor an electron is excited into the conduction band, a bound state with a hole left in the valence band can form. Due to the large dielectric constant of the medium the electron and the hole in the exciton are spatially well-separated. Therefore the electron-hole interaction is a Coulomb attraction modified at short distances. In this context a_B can exceed many times r_0 which is of the order of the Hydrogen Bohr radius.

Zel'dovich was apparently the first to recognize that in the limit $r_0 \ll a_B$ the spectrum of the distorted Coulomb problem is peculiar [3]. Since the centrifugal barrier decreases the probability of particle penetration in the region of small distances r , the effect of the short-range potential is strongest for the states of zero angular momentum. In this case the radial motion of a particle of mass m and energy E in a central potential $U(r)$ is described by the one-dimensional Schrödinger equation [4]

$$\frac{d^2\chi}{dr^2} + \frac{2m}{\hbar^2} (E - U(r)) \chi = 0 \quad (1)$$

where $\chi(r)/r$ is the radial wave function. Zel'dovich chose $U(r) = -\hbar^2/m a_B r$ for $r \geq r_0$ and $U(r) = U_s(r)$

otherwise and demonstrated that as long as the short-range potential $U_s(r)$ is not resonant, its effect is weak. If, on the other hand, $U_s(r)$ has a low-energy scattering resonance, a drastic reconstruction of the spectrum takes place. Using the example of the square well of depth U_0 he stated that as the dimensionless coupling constant $w \simeq m r_0^2 U_0 / \hbar^2$ increases, the spectrum of the problem $E_n(w)$ evolves in a fashion resembling a sharp decreasing staircase. The steps are located at critical values of w at which bound states occur in $U_s(r)$ *only*. As w goes through the first threshold, the Coulomb levels E_n ($n \geq 2$) quickly fall to E_{n-1} while the ground state E_1 rapidly drops downward. The relative width of the region where the spectrum reconstruction takes place, $\Delta w/w \simeq r_0/a_B \ll 1$, is narrow, and qualitatively the same pattern repeats itself upon passing through every subsequent resonance.

A similar spectral behavior has been found by Popov [5] in his analysis of the Dirac equation for an electron in a field of the bare nucleus of charge Ze with $Z > 137$.

The Zel'dovich effect has been re-discovered in the spectra of hadronic atoms, and its generality has been demonstrated for any interaction with two widely different spatial scales [6].

Various aspects of the spectrum reconstruction have been investigated by Popov and collaborators [7]. Their study was motivated by then existing experimental evidence of the large $1s$ -level shift in the proton-antiproton atom which was naturally linked to the Zel'dovich effect. Later it became clear that the experimental level shifts are small and the interest in the phenomenon declined.

As far as we know, at this time there is no documented experimental evidence of the Zel'dovich effect. This is not surprising because the spectrum reconstruction takes place in a narrow range of parameters in the vicinity of low-energy resonances. However a given experimental system is unlikely to be near resonance. A systematic search for the Zel'dovich effect would consist in looking

for spectral changes in response to tuning of the central part of the potential which is often impossible - the strength of the nuclear force cannot be changed in the laboratory.

Recently Karnakov and Popov [8] pointed out that the Zel'dovich spectrum reconstruction takes place for a Hydrogen atom as a function of the external magnetic field thus providing an example of a system where a systematic search for the effect might be possible. Although the phenomenon is observable in numerical studies, direct experimental evidence is lacking and may only come from astrophysical observations as the pertinent magnetic fields are comparable to those on the surface of a neutron star.

The goal of this paper is to demonstrate that evolution of the Rydberg spectra of ordinary atoms along the Periodic Table provides direct evidence of the Zel'dovich effect. Since the condition $r_0 \ll a_B$ does not hold in atomic systems, the way the phenomenon manifests itself is less dramatic - we will show that it can be seen as a systematic periodic spectral modulation as a function of the cubic root of atomic number Z .

It is known that for a highly excited s electron of a Rydberg atom the effect of polarization of the ionic core is negligible compared to that of the wave function penetration in the central region of the atom [9]. Therefore the electron dynamics can be adequately described by Eq.(1) where the effective central field $U(r)$ at large distances is that of a positively charged ion of charge e . On the other hand, starting from distances of the order of the size of the ionic core $r_0 \simeq a_B$ the field felt by the electron begins to deviate from the $-e^2/r$ form on-average decreasing, as $r \rightarrow 0$, to $-Ze^2/r$. By increasing Z along the Periodic Table Nature systematically deepens the inner part of the potential leaving the outer $-e^2/r$ tail intact. Thus by analyzing the Rydberg spectra as a function of atomic number Z it may be possible to correlate them with the binding properties of the ionic core which will constitute evidence of the Zel'dovich effect.

In atomic physics the motion of an electron in the field of a residual atomic ion has been studied in the past. Approximating the potential of the ionic core by that of the Thomas-Fermi or Thomas-Fermi-Dirac theories Latter [10] computed numerically the single-electron term values from $1s$ to $7d$ for all atoms. His ns spectra as a function of atomic number Z for largest n studied clearly show modulations on a decreasing energy curve. It is well-known that the large n atomic spectra are described by the Rydberg formula [9]

$$E_n = -\frac{\hbar^2}{2ma_B^2} \frac{1}{(n-\mu)^2} \quad (2)$$

where μ is the quantum defect which in the limit $n \rightarrow \infty$ does not depend on n . Latter's results imply that the dependence of the quantum defect μ on Z has modulations superimposed on an increasing curve.

The $\mu(Z)$ dependence has been numerically computed by Manson [11] and by Fano, Theodosiou and Dehmer

[12] who used the Hartree-Slater model [13] to approximate the potential of the ionic core of the atom. Although the periodic variations of $\mu(Z)$ are strongly obscured by the shell effects (included in the Hartree-Slater model), Fano, Theodosiou and Dehmer argued that they are there and that there is a correlation between the location of radial nodes of the function χ from Eq.(1) near r_0 and the slope of the $\mu(Z)$ dependence. In view of the oscillation theorem [4] the nodal structure of the function χ is intimately related to the binding properties which suggests that systematic periodic variations of Rydberg spectra as function of Z might be related to the Zel'dovich effect.

In order to demonstrate that this connection is correct below we compute the upper part of the spectrum of the modified Coulomb problem not assuming that $r_0 \ll a_B$. We show that the staircase reconstruction taking place for $r_0 \ll a_B$ and the spectral modulations for $r_0 \simeq a_B$ are different limiting cases of the same phenomenon - sensitivity to the binding properties of the inner part of the potential which we continue to call the Zel'dovich effect. We also compare our results for $\mu(Z)$ with available experimental and numerical data to show that the phenomenon is observable.

The organization of this paper is as follows. In Section II we provide a short derivation of the Rydberg formula (2) and arrive at the expression for the quantum defect in terms of the dimensionless range of the inner potential and its scattering length. This general result is further analyzed in the $r_0 \ll a_B$ limit and the main features of the Zel'dovich spectral reconstruction are recovered (Section IIA). In Section IIB we establish a relationship between the Zel'dovich effect and Levinson's theorem of quantum mechanics. This is followed (Section IIC) by the analysis of the opposite $r_0 \gg a_B$ limit where we demonstrate that the Zel'dovich effect manifests itself in the form of a spectral modulation whose origin still lies in the binding properties of the inner potential $U_s(r)$. These general findings are illustrated in Section IID where we use the exactly-solvable example of the rectangular well as a model for the inner potential. In Section IIE we observe that only a treatment more accurate than semiclassical can capture the Zel'dovich effect.

Section III focuses on the computation of the systematic quantum defect of the Rydberg electron as a function of atomic number Z . First (Section IIIA), for the inner potential having an attractive Coulombic singularity at the origin, we derive a semiclassical expression for the quantum defect and show that it is equal to the number of de Broglie's half-waves fitting inside the inner potential minus a contribution proportional to $(r_0/a_B)^{1/2}$. Going beyond the semiclassical approximation we also demonstrate that the Zel'dovich modulation of the quantum defect is a periodic function of the number of de Broglie's half-waves fitting inside the ionic core of the atom. This is followed by an explicit calculation based on Latter's model of the ionic core [10]. First, the semiclassical quantum defect is calculated as a function of $Z^{1/3}$ (Section

IIIB). Then (in Section IIIC) a full computation capturing the Zel'dovich effect is performed. An important ingredient here is an approximate calculation of the scattering length of the ionic core of the atom. Both the scattering length and the related Zel'dovich modulation of the quantum defect turned out to be nearly periodic functions of $Z^{1/3}$.

In Section IV the results of our systematic calculation are compared with experimental and numerical data. First, we observe that the bulk of the quantum defect values is well-captured semiclassically. Then (Section IVA) we demonstrate that the gross features of the deviation away from semiclassics are due to the effects of the shell structure. This is done by establishing and demonstrating a correlation between the variation of the radius of the ionic core of the atom and corresponding variation of the quantum defect. Finally, in Section IVB a Fourier analysis of the quantum defect variation with $Z^{1/3}$ is conducted which singles out the Zel'dovich effect. As a by-product we also find a $Z^{1/3}$ periodic contribution coming from the shell effects.

We conclude (Section V) by outlining our main result and directions of future work.

II. DISTORTED COULOMB PROBLEM AND QUANTUM DEFECT

We will be interested in the low energy bound states with the classical turning point being far away from the boundary of the central region, i. e. $\hbar^2/ma_B|E| \gg r_0$. Then the quickest way to derive the spectrum is via semiclassical arguments derived from those given by Migdal [14]:

For $r_0 < r < \hbar^2/ma_B|E|$ the semiclassical solution to Eq.(1) can be written in two equivalent forms:

$$\begin{aligned} \chi_{sc} &\propto \frac{1}{\sqrt{p}} \sin \left(\frac{1}{\hbar} \int_r^{\hbar^2/ma_B|E|} pdr + \frac{\pi}{4} \right) \\ &\propto \frac{1}{\sqrt{p}} \sin \left(\frac{1}{\hbar} \int_{r_0}^r pdr + \alpha \right) \end{aligned} \quad (3)$$

where $p = (-2m|E| + 2\hbar^2/ra_B)^{1/2}$ is the momentum. The first representation in Eq.(3) is the standard result with the phase of $\pi/4$ improving on the deficiency of the semiclassical approximation near the classical turning point, while the yet undetermined phase α in the second representation in Eq.(3) both corrects for the failure of the semiclassical approximation in a Coulomb field at distances $r \lesssim a_B$ and accounts for the short-range potential $U_s(r)$.

For $r_0 < r \ll \hbar^2/ma_B|E|$ the Schrödinger equation (1) simplifies to

$$\frac{d^2\chi}{dr^2} + \frac{2}{ra_B}\chi = 0 \quad (4)$$

and can be exactly solved:

$$\chi \propto r^{1/2} \left(J_1(\sqrt{8r/a_B}) - Y_1(\sqrt{8r/a_B}) \tan \delta \right) \quad (5)$$

where $J_\nu(x)$ and $Y_\nu(x)$ are the order ν Bessel functions of the first and second kind respectively [15]. The solution (5) is a linear combination of the regular $J_1(0) = 0$ and irregular $Y_1(0) = \infty$ Coulomb functions of zero energy, and for the purely Coulomb problem, $U_s(r) = -\hbar^2/ma_B r$, one has to recover $\tan \delta = 0$.

For $a_B \ll r \ll \hbar^2/ma_B|E|$ the semiclassical approximation is accurate, and the second representation of Eq.(3) yields $\chi \propto r^{1/4} \sin(\sqrt{8r/a_B} - \sqrt{8r_0/a_B} + \alpha)$. On the other hand, the $r \gg a_B$ limit of (5) is $\chi \propto r^{1/4} \sin(\sqrt{8r/a_B} - \pi/4 + \delta)$ which determines α in (3) to be $\sqrt{8r_0/a_B} - \pi/4 + \delta$. It also implies that δ in (5) is the zero-energy phase shift due to the small-distance deviation of the potential from the Coulomb form.

The energy spectrum can be found from the requirement that the semiclassical expressions (3) coincide. Combined with $\alpha = \sqrt{8r_0/a_B} - \pi/4 + \delta$ this gives the quantization rule

$$\frac{1}{\hbar} \int_{r_0}^{\hbar^2/ma_B|E|} pdr = \pi n - \delta - x_0 \quad (6)$$

where dimensionless parameter

$$x_0 = \sqrt{\frac{8r_0}{a_B}} \quad (7)$$

measures the range of the short-range forces. Calculating the integral we arrive at Eq.(2) with $\delta = \pi\mu$ which is the statement of Seaton's theorem [9] relating the quantum defect to the zero-energy phase shift.

The range of applicability of Eq.(2), $n - \mu \gg (r_0/a_B)^{1/2} \simeq x_0$, follows from the condition $|E| \ll \hbar^2/ma_B r_0$ which also implies that in order to calculate the quantum defect entering the spectrum (2), we only need to match (5) with its zero energy counterpart at $r < r_0$.

We proceed by computing $h = [d \ln \chi / d \ln r]_{r \rightarrow r_0+0}$, the logarithmic derivative of the function (5) evaluated at the boundary of the inner region:

$$h = \frac{x_0 J_0(x_0) - Y_0(x_0) \tan \pi\mu}{2 J_1(x_0) - Y_1(x_0) \tan \pi\mu} \quad (8)$$

where we used $\delta = \pi\mu$. The quantum defect μ is determined by equating (8) to $h_s = [d \ln \chi / d \ln r]_{r \rightarrow r_0-0}$ which can be found by solving the $E = 0$ Schrödinger equation (1) for $r < r_0$ with $U(r) = U_s(r)$:

$$\frac{d^2\chi}{dr^2} - \frac{2m}{\hbar^2} U_s(r)\chi = 0 \quad (9)$$

The parameter h_s can be equivalently expressed in terms of the scattering length corresponding to the inner potential *only*. Indeed for motion in a short-range potential

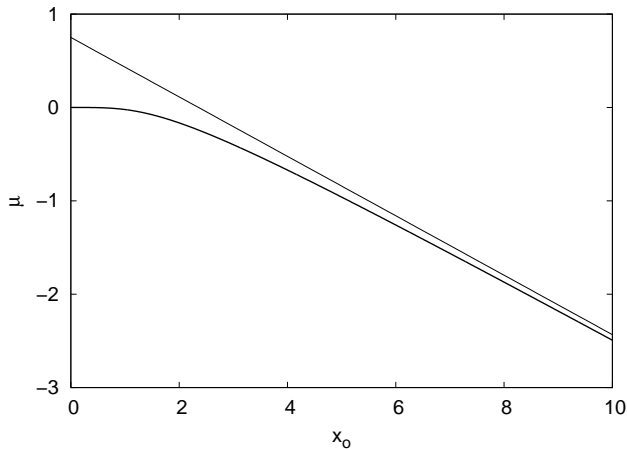


Figure 1: Quantum defect for $U_s(r) = 0$ as a function of the range parameter x_0 , Eq.(7), and its $x_0 \gg 1$ limit, $\mu(0, x_0) = 3/4 - x_0/\pi$ (shown in gray scale).

the scattering length a_s is defined from the asymptotic $r \rightarrow \infty$ behavior $\chi(r) \propto 1 - r/a_s$ of the solution to (9). For a potential well identically vanishing for $r > r_0$, this is also the exact behavior outside the well with the implication that [3, 7]

$$h_s^{-1} = \left(\frac{d \ln \chi(r \rightarrow r_0 - 0)}{d \ln r} \right)^{-1} = 1 - \frac{a_s}{r_0} \quad (10)$$

Then substituting $h = h_s$ in Eq.(8) and using (10) we arrive at the formula for the quantum defect

$$\tan \pi \mu = \frac{2x_0^{-1} J_1(x_0) + (a_s/r_0 - 1) J_0(x_0)}{2x_0^{-1} Y_1(x_0) + (a_s/r_0 - 1) Y_0(x_0)} \quad (11)$$

If the short-distance potential is selected in the form $U_s(r) = -\hbar^2/ma_B r$, i. e. we have the ordinary Coulomb problem in the whole space, the quantum defect μ entering the Rydberg formula (2) must vanish identically. It is straightforward to verify that this is indeed the case: the $E = 0$ inner $r < r_0$ solution to (1), $\chi \propto r^{1/2} J_1(\sqrt{8r/a_B})$, leads to the expression for the scattering length nullifying the numerator of (11). This argument defines the zero of the quantum defect and implies that μ is necessarily positive if for all $r \leq r_0$ the inner potential $U_s(r)$ is more attractive than the Coulomb potential $-\hbar^2/ma_B r$; otherwise the quantum defect is negative. For example, for $U_s(r) = 0$ the quantum defect $\mu(0, x_0)$ is a negative monotonically decreasing function of x_0 such as $\mu = -x_0^4/32$ for $x_0 \ll 1$, and $\mu = 3/4 - x_0/\pi$ in the opposite $x_0 \gg 1$ limit. The $\mu(0, x_0)$ dependence as well as its $x_0 \gg 1$ limit are shown in Fig. 1.

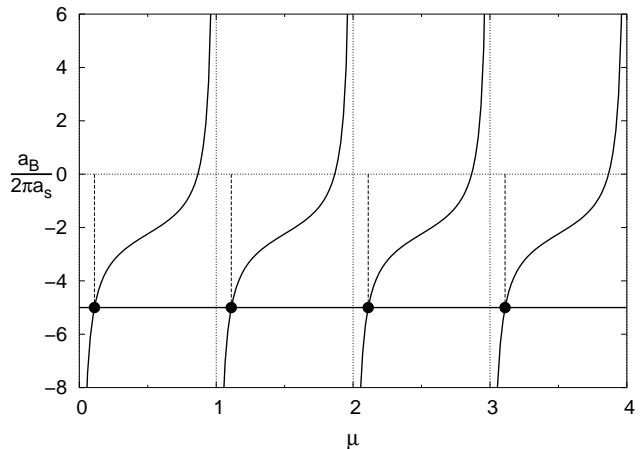


Figure 2: Graphical solution of Eq.(12); $x_0 = 1/30$ has been used to construct the graph. The quantum defect μ is given by the intersections of the right-hand side of (12) with the line of constant $a_B/2\pi a_s$.

A. Zel'dovich effect in the $r_0 \ll a_B$ limit

For $x_0 \ll 1$ Eq.(11) simplifies to a form accumulating the physics of the Zel'dovich effect:

$$\frac{a_B}{2\pi a_s} \equiv \frac{4}{\pi x_0^2 (1 - h_s^{-1})} = -\cot \pi \mu - \frac{2}{\pi} \ln \frac{2}{\gamma x_0} \quad (12)$$

where $\ln \gamma = 0.5772$ is Euler's constant. Terms of higher order in x_0 which for $U_s(r) = 0$ lead to small negative values of the quantum defect are neglected in (12).

We verified that Eq.(12) matches the upper portion of the ns spectrum which for $r_0 \ll a_B$ is known in closed form for any n [7]. We also note that with some effort Eq.(12) can be deduced from the expression for the phase shift of the proton-proton scattering given by Landau and Smorodinskii [16]: in their formula we have to (i) reverse the sign of the Bohr radius, (ii) take the limit of zero energy, and (iii) employ Seaton's theorem [9] $\delta = \pi \mu$.

Fig. 2 shows the dependence of $a_B/2\pi a_s$ on μ given by Eq.(12); its inverse $\mu(a_B/2\pi a_s)$ is a multivalued function consisting of a series of increasing step-like curves sandwiched between nearest non-negative integers. The slope of $\mu(a_B/2\pi a_s)$ is small everywhere except for the vicinity of half-integer μ .

Since typically the central potential $U_s(r)$ is not resonant, $|h_s|$ in (12) is not small. Then the magnitude of the scattering length is of the order of the size of the inner well, $|a_s| \simeq r_0$ and $a_B/2\pi|a_s| \simeq 1/x_0^2$ is significantly larger than the last term in (12). This implies that the quantum defect is very close to an integer, $\mu = -2a_s/a_B \pmod{1}$, with $|a_s|/a_B \simeq r_0/a_B \ll 1$. This conclusion is in quantitative agreement with the results of perturbation theory in a_s/a_B when the deviation from the Bohr Hydrogen formula is small [3, 17]. It is applicable to an attractive non-resonant well of arbitrary strength; for weak $U_s(r)$ which cannot support a bound

state we have $\mu = -2a_s/a_B > 0$ [18] represented by the leftmost intersection in Fig. 2. We also note that the spectrum is exactly Hydrogenic if the scattering length is zero which can be viewed as an analog of the Ramsauer effect [19]: in the present context it refers to a resonant phenomenon when the distortion of the Coulomb potential at small distances is invisible to the low-energy bound (or incident) particle.

Exactly at half-integer μ the scattering length is negative with the magnitude $|a_s| = (a_B/4) \ln^{-1}(2/\gamma x_0) = 2r_0 x_0^{-2} \ln^{-1}(2/\gamma x_0)$ significantly exceeding the size of the central region r_0 . This implies that the slope of the $\mu(a_B/2\pi a_s)$ dependence is largest when $U_s(r)$ itself is almost resonant so that it supports a low-energy *virtual* state. At the point of the steepest slope we also have $[d\chi/dr]_{r=r_0} \propto h_s \simeq (x_0^2/2) \ln(2/\gamma x_0) \ll 1$. Since this is practically zero, one can equivalently say that the slope of the $\mu(a_B/2\pi a_s)$ dependence is largest when the antinode of the function χ in Eq.(1) occurs at the boundary of the inner region r_0 . This criterion resembles that given by Fano, Theodosiou and Dehmer [12] for the dependence of the quantum defect μ on atomic number Z . We note however, that for a Rydberg atom the size of the residual ion does not satisfy the condition $r_0 \ll a_B$; this issue is further addressed below.

If for all r the central well is attractive, its effect can be quantified by a single dimensionless coupling constant $w \simeq mr_0^2|U_s|/\hbar^2 > 0$ where $|U_s|$ has a meaning of the characteristic depth of the well. Then the inverse scattering length a_s^{-1} is known to be a monotonically increasing function of w [7] - an a_s dependence shown in Fig. 3 in gray scale is typical and may help illustrate the argument given below.

The step-like features of the function $\mu(a_B/2\pi a_s)$ are amplified in the $\mu(w)$ dependence. Indeed, for $w \ll 1$ the scattering length a_s is very small and negative. Then the line of constant $a_B/2\pi a_s$ in Fig. 2 lies at very large negative values, the quantum defect satisfies $\mu = -2a_s/a_B \ll 1$, and the deviation from the normal Hydrogen spectrum is small. As the well deepens, the coupling constant w increases, the scattering length becomes more negative and the horizontal line of constant $a_B/2\pi a_s$ moves upward. However as long as the well remains non-resonant, the quantum defect μ will only grow very little. The strongest increase of $\mu(w)$ in response to deepening of the well (and thus the largest deviation from the Bohr Hydrogen formula) occurs when the scattering length reaches a very large negative value $a_s = -2r_0 x_0^{-2} \ln^{-1}(2/\gamma x_0)$. For $x_0 \ll 1$ this takes place very close to a threshold value of the coupling constant w when the first bound state is about to appear in $U_s(r)$. The relative width of the reconstruction region $\Delta w/w$ centered around $\mu = 1/2$ thus can be estimated from the scaling behavior of the scattering length near the threshold $a_s \simeq r_0 w/\Delta w$ and the condition $a_B \simeq |a_s|$. This leads to the original result of Zel'dovich [3] $\Delta w/w \simeq r_0/a_B$.

As the coupling constant w increases through the first binding threshold, the inverse scattering length changes

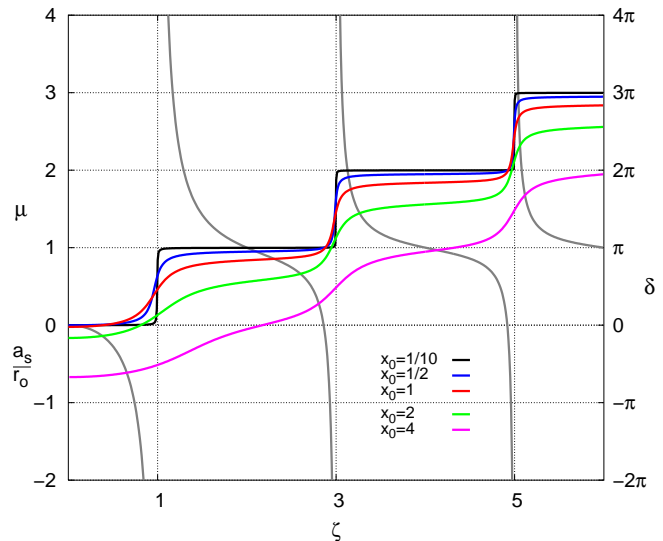


Figure 3: Evolution of the Zel'dovich effect for the rectangular well of radius r_0 and depth U_0 for a series of range parameters x_0 , Eq.(7), manifested in the dependences of the quantum defect μ on $\zeta = (8mU_0r_0^2/\pi^2\hbar^2)^{1/2} \simeq w^{1/2}$. The correlation with the binding properties of the well is seen from the plot of the reduced scattering length a_s/r_0 (gray scale). Shown are also the values of the zero-energy phase shift $\delta = \pi\mu$ relating the Zel'dovich effect to Levinson's theorem.

sign, and the line of constant $a_B/2\pi a_s$ in Fig. 2 enters the region of positive values. After passing through the reconstruction region, the positive scattering length decreases in magnitude, for $a_s/a_B \ll 1$ the quantum defect is close to unity, $\mu = 1 - 2a_s/a_B$, and the deviation from the normal Hydrogen spectrum is again small. In the region $a_s \simeq r_0$ the scattering length does not vary strongly with the depth of the well, and one can say that the slope of the $\mu(w)$ dependence will be minimal when the node of the function χ in Eq.(1) is near the boundary of the central region r_0 which parallels the criterion of Fano, Theodosiou and Dehmer [12]. Upon further increase of the coupling constant w , the scattering length gets smaller and the line of constant $a_B/2\pi a_s$ in Fig. 1 enters the region of very large positive values becoming infinite at $a_s = 0$.

To summarize, as $a_s(w)$ goes through one complete cycle decreasing from zero, passing through the binding resonance, and then approaching zero from above, the quantum defect $\mu(w)$ increases from zero to unity in a staircase fashion: it is mostly zero or unity except for the narrow region $\Delta w/w \simeq r_0/a_B \ll 1$, $\mu \simeq 1/2$ near the first binding threshold of $U_s(r)$. Combined with the Rydberg formula (2) this implies that the Coulomb levels E_n quickly fall to E_{n-1} which constitutes the essence of the Zel'dovich effect [3].

As the coupling constant w continues to increase away from $a_s(w) = 0$, the next cycle, $1 < \mu(w) < 2$, begins and qualitatively same pattern repeats itself. This remains true for every subsequent cycle with $\mu(w)$ sandwiched

between nearest integers. Overall the quantum defect is an increasing function of w having the form of a staircase with practically integer plateaus and sharp steps located at half-integer μ . The steps correspond to the presence of the low-energy scattering resonances in $U_s(r)$.

To illustrate this behavior we choose the inner potential in the form of a rectangular well of depth U_0 whose scattering length is given by $a_s/r_0 = 1 - 2 \tan(\pi\zeta/2)/\pi\zeta$ with dimensionless parameter $\zeta = (8mU_0r_0^2/\pi^2\hbar^2)^{1/2} \simeq w^{1/2}$ quantifying the depth of the well. The scattering length diverges at odd values of ζ which correspond to consecutive occurrences of bound states in the well; the respective dependence of a_s/r_0 on ζ is shown in Fig. 3 in gray scale. We also plot the dependences of the quantum defect μ on ζ found from the general expression (11) for a series of representative x_0 . The analysis based on Eq.(12) is illustrated by the $x_0 = 1/10$ and $x_0 = 1/2$ curves; the latter corresponds to the case of the proton-antiproton atom [7]. These dependences have the form of staircases with nearly integer plateaus; the steepness of the steps where the quantum defect varies by unity and the flatness of the plateaus increase as x_0 gets smaller. An inspection reveals that the points of maximal slope of $\mu(\zeta)$ somewhat precede the scattering resonances in accordance with the analysis given above. This is seen most clearly for the $\zeta \simeq 1$ step of the $x_0 = 1/2$ curve. Fig. 2 of Zel'dovich's work [3] has this feature as well. From a practical standpoint the steps can be considered to coincide with the binding resonances of the well.

The relative width of the reconstruction region $\Delta\zeta/\zeta$ can be estimated as $r_0/a_B\zeta^2$. Since the threshold values ζ grow linearly with the number of bound states, then for fixed x_0 the steepness of the steps increases with ζ as can be seen in Fig. 3. This is merely the consequence of the sharpening of the binding resonances. Similarly the flatness of the plateaus improves as ζ increases, and the points of least slope of the $\mu(\zeta)$ dependence asymptotically approach even values of ζ . This is where the node of the function χ in Eq.(1) coincides with the boundary of the central region, $a_s = r_0$.

Finally we note that the quantum defect takes on exactly integer values whenever the scattering length vanishes.

B. Connection to Levinson's theorem

There is a deep parallel between the Zel'dovich reconstruction of the upper $E \rightarrow 0$ part of the Coulomb spectrum in the $r_0 \ll a_B$ limit and the low-energy scattering by a short-range potential well. For a particle of energy $E = \hbar^2k^2/2m$ whose wave vector \mathbf{k} is small in magnitude, $kr_0 \ll 1$, scattered by the short-range potential $U_s(r)$ vanishing for $r > r_0$ the scattering length a_s can be defined [20] through the $k \rightarrow 0$ limit of the relationship

$$1/ka_s = -\cot\delta_s(k) \quad (13)$$

where $\delta_s(k)$ is the phase shift. Employing Seaton's theorem [9] $\delta = \pi\mu$ relating the quantum defect to the zero-energy phase shift it is straightforward to realize that Eqs.(12) and (13) are direct analogs. The Coulomb field is characterized by its own length scale, the Bohr radius a_B . Its free particle counterpart entering Eq.(13) is the de Broglie wavelength $2\pi/k$. The range of applicability of Eq.(12) $r_0 \ll a_B$ parallels the low-energy condition $kr_0 \ll 1$ necessary for Eq.(13) to hold. The analysis which led to the explanation of the Zel'dovich effect can be repeated for Eq.(13) with the conclusion that the phase shift $\delta_s(k)$ as a function of the dimensionless depth w of the scattering well has the form of a sharp increasing staircase whose plateaus practically coincide with $\delta_s(k) = 0 \pmod{\pi}$. The steps where the phase shift changes by π are very narrow, $\Delta w/w \simeq kr_0 \ll 1$, and the points of steepest slope are located at $\delta_s(k) \simeq \pi/2 \pmod{\pi}$. In the limit $k \rightarrow 0$ the staircase becomes perfect. This can be recognized as Levinson's theorem [20] relating the number of bound states in a well with the zero-energy scattering phase shift. We conclude that for $r_0 \ll a_B$ the Zel'dovich effect expressed in terms of the zero-energy phase shift δ is the Coulombic cousin of Levinson's theorem [21]. A special case of this correspondence, the Ramsauer-like recovery of the normal Hydrogen spectrum for $a_s = 0$, was already mentioned earlier. In the limit $x_0 = \sqrt{8r_0/a_B} \rightarrow 0$ Zel'dovich's staircase becomes perfect and identical to Levinson's staircase. This can be understood as a result of taking the neutral limit, $a_B \rightarrow \infty$, when the Coulomb part of the binding potential $U(r)$ in (1) vanishes. From this viewpoint, Levinson's theorem is a consequence of the Zel'dovich effect. To emphasize the connection to Levinson's theorem, in Fig. 3 we additionally show the zero-energy phase shift $\delta = \pi\mu$.

Fig. 3 also demonstrates that as x_0 increases, the staircase $\mu(\zeta)$ dependence with well-defined steps and plateaus evolves into an increasing function with modulations: the "plateaus" develop noticeable slope and the "steps" acquire a width. Moreover for sufficiently large $x_0 \gtrsim 1$ the staircase-like appearance seems to emerge only for a sufficiently deep well, i. e. large ζ . Another feature is the presence of a negative offset which is a growing function of x_0 . This is due to the fact that for $U_s(r) = 0$ the quantum defect is a monotonically decreasing negative function of x_0 as shown in Fig. 1.

C. Zel'dovich effect in the $r_0 \gg a_B$ limit

In the $x_0 \gg 1$ limit Eq.(11) simplifies to the form

$$\frac{a_s}{r_0} = \frac{2}{x_0} \cot(\pi\mu + x_0 - \frac{3\pi}{4}) + 1 \quad (14)$$

allowing model-independent treatment. The analysis of Eq.(14) is convenient to conduct in terms of the reduced quantum defect $M = \mu + x_0/\pi - 3/4$ whose zero gives the $x_0 \gg 1$ asymptotic of μ for $U_s(r) = 0$. Eq.(14) can be

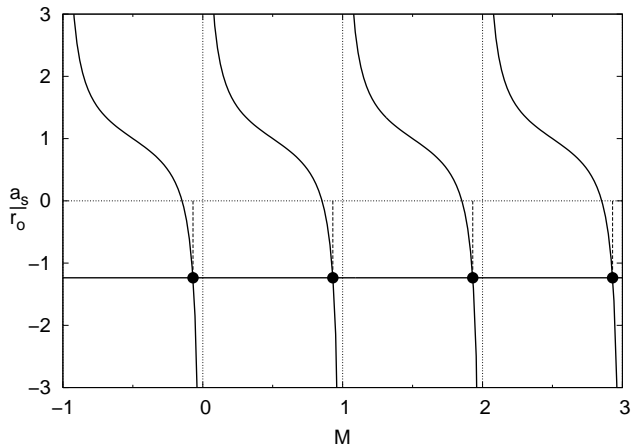


Figure 4: Graphical solution of Eq.(14); $x_0 = 4$ has been used to construct the graph. The reduced quantum defect $M = \mu + x_0/\pi - 3/4$ is given by the intersections of the right-hand side of (14) with the line of constant a_s/r_0 .

investigated in a manner analogous to that of Eq.(12); a brief summary is given below.

Fig. 4 shows the dependence of a_s/r_0 on $M = \mu + x_0/\pi - 3/4$ given by Eq.(14); its inverse $M(a_s/r_0)$ is a multivalued function consisting of a series of decreasing step-like segments sandwiched between nearest integers.

The magnitude of the slope of $M(a_s/r_0)$ is smallest at integer M which occurs at binding resonances, $a_s = \pm\infty$, i. e. when the antinode of the function χ in Eq.(1) coincides with the boundary of the inner region r_0 . In the vicinity of integer M we find $M = 2r_0/\pi x_0 a_s \pmod{1}$. This translates into an explicit result for the quantum defect $\mu = 3/4 - x_0/\pi + 2r_0/\pi x_0 a_s \pmod{1}$ valid in the limit $x_0 \gg 1$ and $r_0/x_0 a_s \ll 1$, thus roughly covering the range of $|a_s|$ from r_0 to infinity. In the vicinity of the first binding resonance we have $\mu = 3/4 - x_0/\pi + 2r_0/\pi x_0 a_s$ which is represented by the leftmost intersection in Fig. 4.

The magnitude of the slope of the $M(a_s/r_0)$ dependence is largest at half-integer M which occurs at $a_s = r_0$, i. e. when the node of the function χ in Eq.(1) coincides with the boundary of the inner region r_0 . Since the reduced quantum defect M is a decreasing function of a_s/r_0 , and the scattering length a_s is a decreasing function of the well depth w [7], then for fixed x_0 the parameter M (and thus the original quantum defect μ) is an increasing function of w .

In contrast to the $x_0 \ll 1$ regime, here the step-plateau features of the function $M(a_s/r_0)$ are generally suppressed in the $M(w)$ dependence. This is because the dependence of the scattering length a_s on the depth of the well w is weakest in the region $a_s \simeq r_0$ where the $M(a_s/r_0)$ dependence shows a “step”. By the same token the “plateaus” acquire a noticeable slope since the $a_s(w)$ dependence is strongest near the binding resonance, $a_s = \pm\infty$, i. e. where the $M(a_s/r_0)$ dependence is weakest. As a result the dependence of the quantum

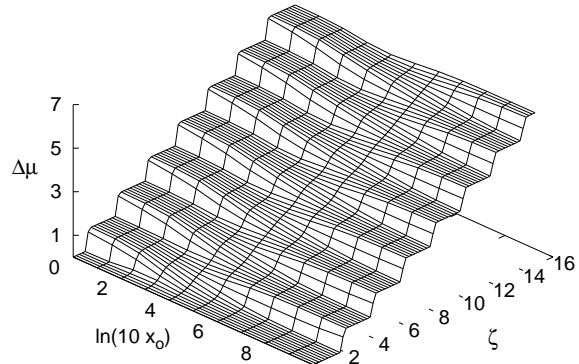


Figure 5: Plot of the surface of the relative quantum defect $\Delta\mu(\zeta, x_0) = \mu(\zeta, x_0) - \mu(0, x_0)$ for a rectangular potential well with dimensionless range and depth parameters x_0 and ζ , respectively, according to Eq.(11).

defect μ on the depth of the well w is more appropriately viewed as consisting of modulations superimposed on an increasing curve. These modulations still have their origin in the binding properties of the inner potential $U_s(r)$.

D. Rectangular well example

The analysis of Sections IIA and IIC is illustrated in Fig. 5 where using the example of the rectangular well and Eq.(11) we plot the surface of the relative quantum defect $\Delta\mu(\zeta, x_0) = \mu(\zeta, x_0) - \mu(0, x_0)$. The point of subtracting $\mu(0, x_0)$ from $\mu(\zeta, x_0)$ is to isolate the physics of binding from the background $\mu(0, x_0)$ which is a monotonically decreasing function of x_0 shown in Fig. 1. The peculiar shape of the resulting surface can then be understood as follows:

For $x_0 \ll 1$ the background contribution $\mu(0, x_0)$ is negligible (see Fig. 1), the relative quantum defect $\Delta\mu(\zeta, x_0)$ reduces to $\mu(\zeta, x_0)$ which, according to our earlier analysis, is a staircase function of ζ with steps located at odd ζ , i. e. when the bound states occur in the well.

For $x_0 \gg 1$ the background contribution $\mu(0, x_0)$ is $3/4 - x_0/\pi$, and we find that $\Delta\mu(\zeta, x_0) = \mu(\zeta, x_0) - \mu(0, x_0) = \mu(\zeta, x_0) + x_0/\pi - 3/4 = M$ which, according to Fig. 4, is a decreasing staircase function of a_s/r_0 . For not very deep well the dependence on ζ has a form of a rounded staircase with “steps” and “plateaus” centered at even ($a_s = r_0$) and odd ($a_s = \pm\infty$) values of ζ , respectively. In this regime the underlying step-plateau character of the $M(a_s/r_0)$ function is preserved in the $M(\zeta)$ dependence due to the appreciable slope of the $a_s(\zeta)$ dependence at $a_s = r_0$ and relatively weak divergence at $a_s = \pm\infty$. To recapitulate, both for $x_0 \ll 1$ and $x_0 \gg 1$ and not very deep well the relative quantum

defect $\Delta\mu(\zeta, x_0)$ is an increasing staircase function of the depth parameter ζ with the steps located at odd ($x_0 \ll 1$) or even ($x_0 \gg 1$) values of ζ . The crossover between the two regimes can be seen in Fig. 5 as a relatively narrow stripe of very weak modulations.

A qualitatively different staircase-like dependence emerges for $x_0 \gg 1$ and sufficiently deep well because as $\zeta \rightarrow \infty$ the slope of the $a_s(\zeta)$ function at $a_s = r_0$ tends to zero while the binding resonances, $a_s = \pm\infty$, become progressively more singular. As a result the “steps” and “plateaus” switch places - the former becomes centered at odd while the latter at even values of ζ . This is somewhat similar to what happens in the $x_0 \ll 1$ limit. This observation explains why the small modulation crossover stripe in Fig. 5 runs at an angle to the $(\Delta\mu, \zeta)$ plane. The important qualitative difference between the $x_0 \ll 1$ and $x_0, \zeta \gg 1$ staircases is that the latter have “plateaus” centered at half-integer values of M , thus corresponding to the coincidence of a node of the function χ in Eq.(1) with the boundary of the inner region $r = r_0$.

E. Semiclassical treatment

For most realistic models of the inner potential $U_s(r)$ the exact analytical calculation of the scattering length a_s entering the general expression for the quantum defect Eq.(11) may not be possible. Therefore it is pertinent to understand whether there is an approximate analytical treatment capturing the Zel’dovich spectrum reconstruction. This is especially relevant to the $x_0 \gg 1$ regime when the phenomenon manifests itself only as a modulation of the quantum defect superimposed on a monotonic curve.

For $x_0 \gg 1$ and sufficiently smooth $U_s(r)$ the standard semiclassical approximation is applicable, and the corresponding solution to Eq.(9) can be written as

$$\chi_{sc}(r) \sim (S'(r))^{-1/2} \sin \frac{S(r)}{\hbar}, \quad (15)$$

where

$$S(r) = \int_0^r (-2mU_s(r))^{1/2} dr \quad (16)$$

is the classical action acquired by a zero-energy particle moving radially out from zero to r , and the prime in Eq.(15) denotes differentiation with respect to r . The semiclassical expression for the scattering length which can be deduced from Eq. (15) with the help of Eq. (10) has been given by Berry [22]

$$\frac{a_s}{r_0} = 1 - \left(-\frac{\hbar^2}{2mr_0^2 U_s(r_0)} \right)^{1/2} \tan \frac{S_0}{\hbar} \quad (17)$$

where $S_0 \equiv S(r_0)$. Eqs.(15) and (17), generalizing the “rectangular well” expressions for the wave function and

the scattering length, are applicable when the number of de Broglie’s half-waves $S_0/\pi\hbar$ fitting inside $U_s(r)$ is very large. If we additionally assume the continuity of the central potential $U(r)$ in Eq.(1) at the boundary of the inner region,

$$U_s(r_0) = -\hbar^2/ma_B r_0, \quad (18)$$

then Eq.(17) simplifies to $a_s/r_0 = 1 - (2/x_0) \tan(S_0/\hbar)$. Combining this with Eq.(14) we find an explicit semiclassical expression for the quantum defect

$$\mu_{sc} = \frac{3}{4} - \frac{x_0}{\pi} + \frac{S_0}{\pi\hbar} - \frac{1}{2} \quad (19)$$

which can be interpreted as approximately the sum of $3/4 - x_0/\pi$, the quantum defect for $U_s(r) = 0$, and the number of de Broglie’s half-waves $S_0/\pi\hbar$ fitting inside the inner part of the potential; the estimate $\mu_{sc} \simeq S_0/\pi\hbar$ has been given earlier [9]. The number of de Broglie’s half-waves can be estimated in terms of the dimensionless depth of the inner well $w \simeq mr_0^2|U_s|/\hbar^2$ as $S_0/\pi\hbar \simeq w^{1/2}$ which implies that for fixed x_0 the quantum defect (19) is a monotonically increasing function of w without any modulations. We conclude that the Zel’dovich modulations of the quantum defect are lost in the semiclassical approximation despite the fact that the corresponding scattering length (17) does exhibit binding resonances. Thus for $x_0 \gg 1$ a treatment better than semiclassical is required to capture the deviations from monotonic behavior; a similar conclusion has been reached earlier [12].

For the rectangular well of radius r_0 and depth U_0 characterized by the coupling constant $\zeta = (8mU_0r_0^2/\pi^2\hbar^2)^{1/2}$ the expression for the scattering length (17) is exact, and then Eq.(19) predicts that $\mu = 1/4 - x_0/\pi + \zeta/2 = 1/4 - \zeta/2 < 0$. This is the $x_0, \zeta \gg 1$ value of the quantum defect in the middle of the small modulation stripe in Fig. 5 whose locus, $x_0 = \pi\zeta$, can be deduced from Eq.(18). The quantum defect is negative because for continuous $U(r)$ the short-distance rectangular well potential is always less attractive than the Coulomb potential.

III. QUANTUM DEFECT OF RYDBERG ELECTRON

Now when we understand the manifestations of the Zel’dovich effect, and what kind of accuracy is required to approximately capture it, we begin computing the quantum defect of the Rydberg electron as a function of position along the Periodic Table. The quantum defect is given by the exact result Eq.(11) with r_0 and a_s , being the size and the scattering length of the residual atomic ion, respectively, both dependent upon atomic number Z . The resulting $\mu(Z)$ dependence will exhibit modulations both due to systematic (Zel’dovich) and shell effects. As discussed in the Introduction, the shell effects obscure systematic trends making it difficult to see

that some modulations of $\mu(Z)$ have their origin in the binding properties of the ionic core. To circumvent this inconvenience below we conduct a calculation capturing only systematic effects. The comparison of the results with both experimental and numerical data (additionally containing the shell effects) will allow us to disentangle physically different sources of deviation from purely monotonic behavior.

A. Method of comparison equations

The short-distance potential $U_s(r)$ characterizing the residual atomic ion will be assumed to match at its boundary the Coulomb potential of unit charge [10],[12] (see Eq.(18)). As the Rydberg electron moves inside the ionic core, the screening of the nuclear charge by the inner shell electrons diminishes which implies that for $r < r_0$ the short-distance potential $U_s(r)$ is more attractive than the Coulomb potential of unit charge. Therefore the quantum defect is a necessarily positive and increasing function of atomic number Z . As $r \rightarrow 0$, the inner potential approaches that of a nucleus of charge Ze , i. e. $U_s(r \rightarrow 0) \rightarrow -Ze^2/r = -Z\hbar^2/ma_{Br}$, and Eq.(9) reduces to

$$\frac{d^2\chi}{dr^2} + \frac{2Z}{ra_B}\chi = 0 \quad (20)$$

This presents a convenient starting point for obtaining an approximate solution to the differential equation (9) via the method of comparison equations as described by Berry and Mount [23]. Since Eq.(20) is exactly solvable, and the potentials of Eqs.(9) and (20) are somewhat similar, the solution to (9) should be also similar to that of (20) and can be transformed into it by a slight deformation of coordinates and an amplitude adjustment. The details of finding an appropriate mapping are given in Ref. [23]; the resulting approximate solution of (9) is then given by

$$\chi(r) \sim \left(\frac{S(r)}{S'(r)}\right)^{1/2} J_1\left(\frac{S(r)}{\hbar}\right) \quad (21)$$

The method of comparison equations includes the conventional semiclassical treatment as a special case [23]. From this more general viewpoint Eq. (15) can be viewed as a result of the deformation and amplitude adjustment of the ‘‘rectangular well’’ sine solution.

To assess the accuracy of (21) let us first look at the limit $S(r)/\hbar \ll 1$. According to Eq.(16) this corresponds to $r \rightarrow 0$ when $U_s(r) \rightarrow -Z\hbar^2/ma_{Br}$. Then $S(r \rightarrow 0)/\hbar \rightarrow (8Zr/a_B)^{1/2}$ and $\chi(r \rightarrow 0) \sim r^{1/2} J_1(\sqrt{8Zr/a_B})$ which can be recognized as the solution to (20).

In the opposite limit $S(r)/\hbar \gg 1$ a semiclassical approximation is expected to be valid and Eq.(21) simplifies to $\chi(r) \sim (S'(r))^{-1/2} \sin(S(r)/\hbar - \pi/4)$. This is similar to the naive semiclassical result (15) with the extra phase

of $-\pi/4$ correcting for the failure of the standard semiclassical treatment in the Coulomb field of charge Ze at distances $r \lesssim a_B/Z$. Thus for the inner potential $U_s(r)$ which has a Coulombic singularity as $r \rightarrow 0$ but is otherwise smooth the analog of Eq.(19) is

$$\mu_{sc} = -\frac{x_0}{\pi} + \frac{S_0}{\pi\hbar} \quad (22)$$

The expression for the scattering length corresponding to Eq.(21) can be found with the help of Eq.(10)

$$\frac{a_s}{r_0} = 1 - 4 \left(x_0 \left(\frac{\hbar}{S_0} + \frac{J_0(\frac{S_0}{\hbar}) - J_2(\frac{S_0}{\hbar})}{J_1(\frac{S_0}{\hbar})} \right) - \frac{r_0 U'_s(r_0)}{U_s(r_0)} \right)^{-1} \quad (23)$$

where we also used the condition of continuity (18). Eq.(23) can be used to go beyond the semiclassical expression (22). Combining Eqs.(14) and (23) we find that in the $x_0, S_0/\hbar \gg 1$ limit the quantum defect can be presented as $\mu = \mu_{sc} + \delta\mu$ where μ_{sc} is the semiclassical answer (22) and the correction,

$$\delta\mu = \frac{r_0 U'_s(r_0)}{4\pi x_0 U_s(r_0)} \left(1 - \sin \frac{2S_0}{\hbar} \right), \quad (24)$$

captures the Zel’dovich effect now manifesting itself as a simple harmonic modulation superimposed on the semiclassical background. The period of the oscillation is exactly one de Broglie’s half-wave while the amplitude is of the order x_0^{-1} . The fact that the latter is independent of the number of de Broglie’s half-waves fitting inside $U_s(r)$ implies that the Zel’dovich effect persists for any value of $S_0/\pi\hbar$.

B. Thomas-Fermi model of atomic ion: semiclassical solution

Below we follow Latter [10] and assume that the potential of the atomic ion $U_s(r)$ can be approximated by the Thomas-Fermi theory [24]:

$$U_s(r) = -\frac{\hbar^2 Z}{ma_{Br}} \phi\left(\frac{rZ^{1/3}}{ba_B}\right) \quad (25)$$

where $b = (3\pi/4)^{1/2}/2 \simeq 0.885$, and the universal function $\phi(y)$ is the solution to the nonlinear Thomas-Fermi equation

$$y^{1/2} \frac{d^2\phi}{dy^2} = \phi^{3/2} \quad (26)$$

subject to the boundary conditions $\phi(0) = 1$ and $\phi(\infty) = 0$ [24]. Then the size of the ion r_0 and thus the range parameter x_0 (7) are determined by the continuity condition (18), i. e. when the Thomas-Fermi potential (25) meets the Coulomb potential of unit charge:

$$\phi\left(\frac{x_0^2 Z^{1/3}}{8b}\right) = \frac{1}{Z} \quad (27)$$

Eqs. (25) and (27) imply that the natural variable to characterize the strength of the potential of the atomic ion is $Z^{1/3}$. Indeed, the typical length scale of the Thomas-Fermi theory is $a_B/Z^{1/3}$, the magnitude of the typical potential is $(Z\hbar^2/ma_B)(Z^{1/3}/a_B) = (\hbar^2/ma_B^2)Z^{4/3}$, and thus the dimensionless coupling constant $w \simeq mr_0^2|U_s|/\hbar^2$ which entered the general analysis of Section II is of the order $Z^{2/3}$; the parameter $Z^{1/3}$ then parallels $\zeta \simeq w^{1/2}$ used in the rectangular well example of the inner potential.

Since the Thomas-Fermi function $\phi(y)$ is a monotonically decreasing function of its argument, the $x_0(Z^{1/3})$ dependence defined through Eq.(27) is a monotonically increasing function of $Z^{1/3}$. The boundary condition $\phi(0) = 1$ implies that $x_0(1) = 0$ which is in accordance with the expectation that for Hydrogen ($Z = 1$) we have the standard Coulomb problem in the whole space ($x_0 = 0$). As evident from (27) small values of ϕ are relevant for large Z ; in view of $\phi(y \rightarrow \infty) \rightarrow 144/y^3$ [24] this means that there is an upper bound to the range parameter, $x_0(\infty) = 2^{13/6}3^{1/3}b^{1/2} \simeq 6.092$.

Another quantity of interest is the number of de Broglie's half-waves fitting inside the Thomas-Fermi atomic ion

$$\begin{aligned} \frac{S_0}{\pi\hbar} &= \int_0^{r_0} \left(\frac{-2mU_s(r)}{\pi^2\hbar^2} \right)^{1/2} dr \\ &= \frac{(2b)^{1/2}Z^{1/3}}{\pi} \int_0^{x_0^2 Z^{1/3}/8b} \left(\frac{\phi(y)}{y} \right)^{1/2} dy \quad (28) \end{aligned}$$

which is a monotonically increasing function of $Z^{1/3}$: for $Z \rightarrow 1$ it vanishes as x_0/π while for large Z we have $S_0/\pi\hbar \sim Z^{1/3}$, a known result [14].

For intermediate values of the atomic number the $Z^{1/3}$ dependences of the range parameter x_0 and the number of de Broglie's half-waves $S_0/\pi\hbar$ can be found by numerically solving the Thomas-Fermi equation (26), inverting (27), and computing the integral (28). The results are displayed in Fig. 6 where we show x_0/π and $S_0/\pi\hbar$ as functions of $Z^{1/3}$. These functions are used to also plot the semiclassical quantum defect given by Eq.(22). To assess the accuracy of the resulting $\mu_{sc}(Z^{1/3})$ dependence we need to verify whether approximations used to derive Eq.(22) are adequate. The first assumption, $x_0 \gg 1$, is equivalent to the assertion that the quantum defect for $U_s(r) = 0$ can be replaced by its large x_0 limit. Looking at Fig. 1 where the dependences in question are compared we conclude that "large" here really means $x_0 \gtrsim \pi$. The second, semiclassical assumption $S_0/\hbar \gg 1$ in practice has a good accuracy provided $S_0/\pi\hbar$, the number of de Broglie's half-waves fitting into the inner potential $U_s(r)$, is anything more than one or two. Inspecting Fig. 6 we see that the conditions $x_0/\pi \gtrsim 1$ and $S_0/\pi\hbar \gtrsim 2$ are satisfied for $Z \gtrsim 8$. This is also the practical condition for the Thomas-Fermi-Latter model of the residual ion to be applicable. We note additionally that although

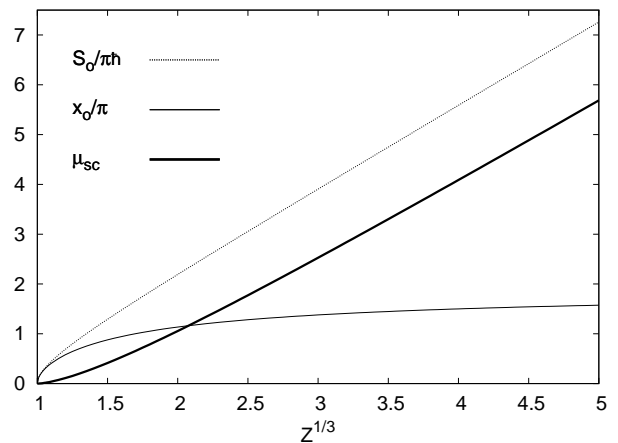


Figure 6: Plots of the number of de Broglie's half-waves $S_0/\pi\hbar$, (28), the range parameter x_0/π , (27), and semiclassical quantum defect μ_{sc} , (22) as functions of $Z^{1/3}$ for the Thomas-Fermi model of the residual atomic ion.

Eq.(22) is not expected to be valid for smallest Z , the limit $\mu(1) = 0$ is nevertheless correctly reproduced and for any Z the semiclassical quantum defect is an increasing positive function of $Z^{1/3}$ in accordance with physical expectation. We conclude that except possibly for the elements of the first row of the Periodic Table, the semiclassical result for the quantum defect Eq.(22) shown in Fig. 6 is accurate; only qualitative agreement is expected for lightest elements.

C. Beyond semiclassical approximation: connection to binding properties of ionic core

A more accurate $\mu(Z^{1/3})$ dependence can be found by computing the scattering length (23) and substituting the outcome together with the $x_0(Z^{1/3})$ dependence, Fig. 6, in our general expression for the quantum defect (11). The result is shown in Fig. 7 where we also plot the semiclassical quantum defect, μ_{sc} , Eq.(22) (gray scale). It now becomes obvious that for any Z the bulk contribution into the quantum defect is well-captured semiclassically. The Zel'dovich spectral modulation clearly visible in Fig. 7 is a relatively weak effect. To separate the modulation from the monotonic semiclassical background the inset shows the difference $\delta\mu = \mu - \mu_{sc}$ which appears to be a nearly periodic function of $Z^{1/3}$. To better understand the meaning of this periodicity the inset also shows the limiting expression (24) (gray scale) [25]. Both curves are exactly in phase and for sufficiently heavy elements their magnitudes agree semi-quantitatively. This observation implies that the Zel'dovich modulation is a periodic function of the number of de Broglie's half-waves fitting inside the ionic core of the atom.

A complementary way to see the connection between the spectral modulation and the binding properties is presented in Fig. 8 where we compare the $\delta\mu(Z^{1/3})$ de-

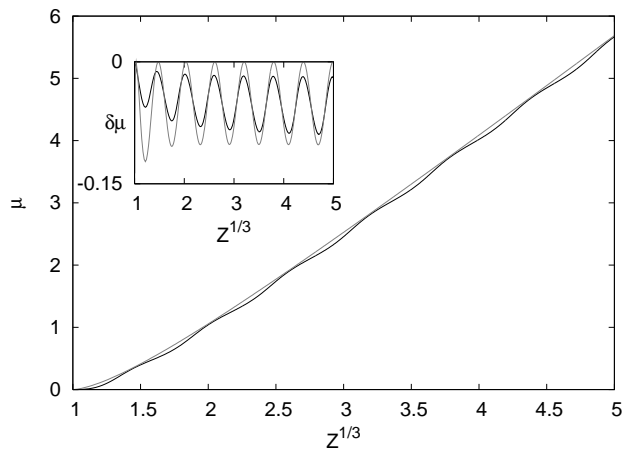


Figure 7: Dependence of the quantum defect μ on $Z^{1/3}$ along with its semiclassical approximant μ_{sc} , Eq.(22) (gray scale). The inset shows the Zel'dovich modulation $\delta\mu(Z^{1/3}) = \mu - \mu_{sc}$ together with the limiting expression, Eq.(24) (gray scale).

pendence with the behavior of the scattering length of the residual atomic ion (23). The latter, numerically computed for the Thomas-Fermi model of the residual atomic ion, Eqs.(25) - (28), is shown in gray scale. The binding singularities of the scattering length are nearly equidistant confirming the earlier observation that the parameter $Z^{1/3}$ is analogous to ζ used in Figs. 3 and 5 to display the Zel'dovich effect for the rectangular well model of the inner potential. A qualitatively similar behavior of the scattering length of the Thomas-Fermi atom as a function of Z has been reported by Robinson [26]; quantitative differences may be attributed to the assumption [26] that the Thomas-Fermi potential vanishes at a distance of the order $a_B/Z^{1/3}$ which is different from our choice of r_0 , Eqs.(18) and (27).

Fig. 8 makes it clear that the maxima of the oscillation $\delta\mu$ occur when $a_s = r_0$, i. e. when the node of the function $\chi(r)$ in Eq.(1) coincides with the boundary of the atomic ion. On the other hand, the minima of $\delta\mu$ are correlated with binding singularities of the ionic core, $a_s = \pm\infty$, thus corresponding to the antinode of $\chi(r)$ being near the ion boundary.

IV. COMPARISON WITH EXPERIMENTAL AND NUMERICAL DATA

We found experimental values of quantum defects for 37 elements of the Periodic Table. These data and their sources are compiled in Table 1 where we also list systematic quantum defects of our work (also displayed in Fig. 7). Some of the figures which we regard as “experimental” came from an on-line database [29] where the quantum defect is computed from available spectroscopic data.

In cases of He, Be, Mg, Ca, and Mo there is more than

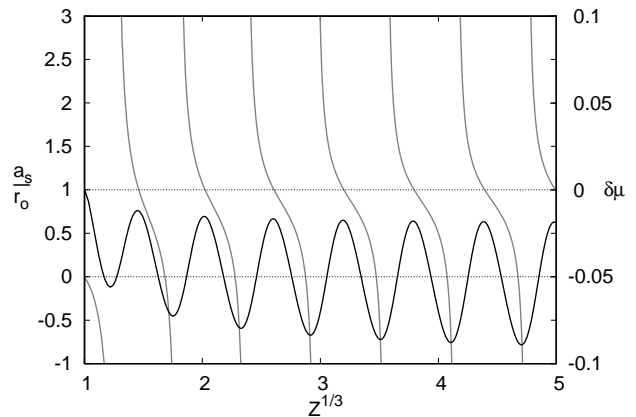


Figure 8: Dependences of the Zel'dovich modulation $\delta\mu = \mu - \mu_{sc}$ and the reduced scattering length of the ionic core a_s/r_0 (gray scale) on $Z^{1/3}$. The lines $a_s/r_0 = 0$ and $a_s/r_0 = 1$ are also shown to help the eye.

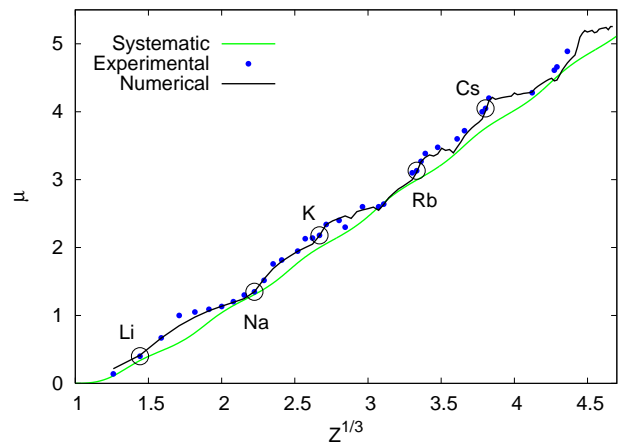


Figure 9: Systematic, experimental, and numerical dependences of the quantum defect μ on $Z^{1/3}$. To help orientation within the Periodic Table experimental alkali data are circled.

one value of the quantum defect available depending on the angular momentum of the ionic core of the atom. Since our theory represents average properties and does not distinguish between different LS terms of an atomic configuration, in Table 1 we chose to show only the values corresponding to lowest angular momentum of the ionic core. It turns out they better agree with our calculation than those left out.

The works of Manson [11] and Fano, Theodosiou and Dehmer [12] contain graphs of numerically evaluated $\mu(Z)$ dependence for all elements. After verifying that the results of both studies are nearly identical, we chose to restrict ourselves to those of the later Ref.[12].

Experimental, numerical and systematic $\mu(Z^{1/3})$ dependences are displayed in Fig. 9. In order to produce the numerical curve, the data [12] have been scanned, digitized, and replotted as a function of $Z^{1/3}$. We also

Table I: Experimentally measured quantum defects for series of elements with their atomic numbers Z and corresponding references. Systematic quantum defects of this work are also displayed for comparison.

Z	Element	Experimental μ	Reference	Systematic μ
2	He	.139	[27]	.110
3	Li	.400	[28]	.336
4	Be	.670	[29]	.478
5	B	1.000	[29]	.600
6	C	1.050	[29]	.744
7	N	1.091	[29]	.904
8	O	1.132	[29]	1.040
9	F	1.203	[29]	1.144
10	Ne	1.300	[30]	1.229
11	Na	1.348	[28]	1.307
12	Mg	1.517	[29]	1.388
13	Al	1.758	[31]	1.476
14	Si	1.816	[29]	1.574
16	S	1.947	[29]	1.774
17	Cl	2.128	[32]	1.861
18	Ar	2.140	[30]	1.935
19	K	2.180	[28]	1.999
20	Ca	2.340	[27]	2.056
22	Ti	2.400	[33]	2.161
23	V	2.300	[33]	2.134
26	Fe	2.600	[33]	2.390
29	Cu	2.600	[27]	2.594
30	Zn	2.639	[34]	2.660
36	Kr	3.100	[30]	2.956
37	Rb	3.131	[35]	2.994
38	Sr	3.269	[27]	3.031
39	Y	3.385	[36]	3.067
42	Mo	3.476	[37]	3.180
47	Ag	3.600	[38]	3.404
49	In	3.720	[39]	3.503
54	Xe	4.000	[30]	3.722
55	Cs	4.049	[40]	3.759
56	Ba	4.200	[27]	3.793
70	Yb	4.280	[27]	4.193
78	Pt	4.611	[36]	4.479
79	Au	4.660	[41]	4.515
83	Bi	4.890	[27]	4.645

circled locations of alkali metals because their ionic cores have noble element electronic configurations thus marking (for the Rydberg atom problem) the end of a period.

Fig. 9 makes it clear that all three dependences are in fairly good agreement and $Z^{1/3}$ is certainly the right variable to use for analysis. It is not surprising that numerical results [12] are generally in better agreement with experimental data than our systematic findings because our calculation omits the shell effects.

A. Effects of shell structure

In order to be able to separate systematic and shell effects, in Fig. 10 we display $\delta\mu = \mu - \mu_{sc}$, the modulation

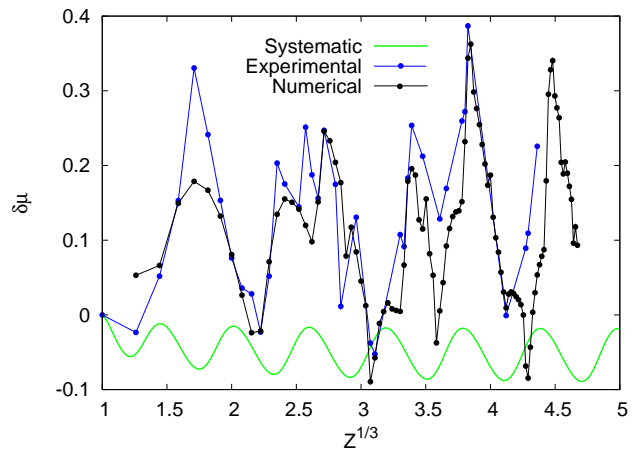


Figure 10: Modulation of systematic, experimental and numerical quantum defect $\delta\mu = \mu - \mu_{sc}$ relative to the semiclassical background, Eq.(22) as a function of $Z^{1/3}$.

of the quantum defect relative to the monotonic semiclassical background, Eq. (22), which accounts for the bulk of the quantum defect value. Fig. 10 shows that the experimental and numerical variations of the quantum defect are bounded which is consistent with the view that they are due to repetitive physics. Moreover, the systematic modulation due to the Zel'dovich effect appears to have an amplitude which is several times smaller than those of experimental and numerical data. This observation implies that it may be possible to understand gross features of the experimental and numerical modulations of the quantum defect as mostly due to the effects of the shell structure.

This viewpoint can be supported by qualitative analysis which rests on the semiclassical result (22). First, let us anticipate the outcome of incorporating the shell effects into the calculation. This amounts to replacing the smooth inner potential $U_s(r)$ by one with modulations due to the spatial variation of the electron density reflecting the shell structure. This replacement will result in a value of the size of the ionic core r_0 , Eq.(18), generally different from its systematic counterpart.

Let us additionally assume that the inner potential $U_s(r)$ with shell effects included is still sufficiently smooth so that a semiclassical treatment is valid. The corresponding quantum defect (22) will deviate away from the systematic result due to different values of the range parameter x_0 , Eq.(7), and the number of de Broglie's half-waves, $S_0/\pi\hbar$. Because the latter involves the integral of $(-U_s(r))^{1/2}$ from zero to r_0 (see Eqs.(16) and (28)) the modulations above and below the systematics present in $U_s(r)$ are expected to largely cancel each other and the deviation from our results can be mostly attributed to the different size of the ionic core.

This argument implies that the quantum defect is strongly sensitive to the value of the size of ionic core r_0 and weakly sensitive to the details of the inner po-

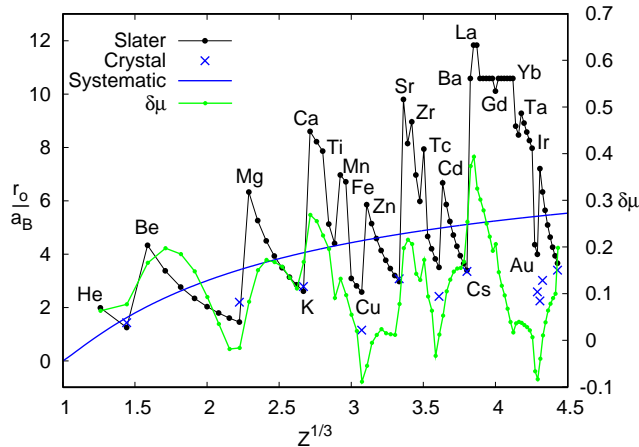


Figure 11: Slater's ionic radii for singly-charged positive ions together with a series of corresponding ionic radii in crystals and systematic sizes of ionic core of the Rydberg atom, all in atomic units, as functions of $Z^{1/3}$. Numerical variation of the quantum defect $\delta\mu = \mu - \mu_{sc}$ is also displayed to show the correlation with Slater's radii.

tential $U_s(r)$. In reality the inner potential may not be smooth enough for the semiclassical treatment to be quantitatively correct. Therefore we do not expect more than a qualitative insight into the trends of the variations of the quantum defect induced by the shell effects.

The simple rule that emerges can be most easily deduced from Fig. 6 by keeping in mind the relationship between the range parameter x_0 , Eq.(7) and the size of the ionic core $r_0 \propto x_0^2$: deviation in r_0 away from systematics leads to the same sign deviation in the quantum defect. Since the size of the ionic core of the Rydberg atom has a physical meaning close to that of an ionic radius, to verify the correlation we need a set of ionic radii for singly-charged positive ions as a function of position Z along the Periodic Table.

Seventy five years ago J. C. Slater [42] gave a very useful, general, empirical set of rules to approximate analytically atomic wave functions for all the elements in any stage of ionization. The radial part of the single-electron wave function is selected in the form

$$\psi(r) \propto r^{n^*-1} e^{-Z^*r/n^*a_B} \quad (29)$$

which can be recognized as the large-distance asymptotics of a Hydrogen-like wave function with an effective quantum number n^* and an effective nuclear charge Z^*e . Based on the underlying electronic structure, Slater's rules assign values of n^* and Z^* to the electrons of each shell of an atom or ion, so that a complete set of single-electron wave functions can be constructed.

For a given shell the maximum of the electron density $4\pi r^2 \psi^2(r)$ is located at

$$r_{max}/a_B = (n^*)^2/Z^* \quad (30)$$

which formally coincides with the expression for the radius of the corresponding circular orbit in Bohr's old the-

ory. The radius of the maximum density of the outermost shell is expected to correlate with the size of the atom or ion. Specifically, Slater defines an ionic radius $r_0 > r_{max}$ as a distance at which the electron density becomes 10% of its maximal value.

Using the existing knowledge of electronic configurations [43] we applied Slater's rules to calculate the ionic radii of singly-charged positive ions. The result is shown in Fig. 11 where the elements marking the beginning or an end of more dramatic changes in the ionic radius are labeled. For comparison we also displayed a series of ionic crystal radii [44] used for predicting and visualizing crystal structures. Crystal ionic radii are based on experimental crystal structure determinations, empirical relationships, and theoretical calculations. As Fig. 11 shows, they are in fair agreement with their Slater's counterparts. We hasten to mention that neither Slater's nor the crystal ionic radii are expected to coincide with what we define as the size of the ionic core of the Rydberg atom, Eq.(18). It seems highly plausible, however, that Slater's ionic radii are correlated with the sizes of ionic core of the Rydberg atom.

Inspection of Fig. 11 tells us that the average Slater's ionic radius slowly grows with $Z^{1/3}$ in fairly good agreement with our systematic result. A closer look reveals that our systematic radius appears to be consistently smaller than its Slater's counterpart. If the same relationship would hold between the systematic and (unknown) exact sizes of ionic cores of Rydberg atoms, then the fact that experimental and numerical quantum defects in Figs. 9 and 10 are generally larger than their systematic counterparts would be explained.

The large variation of the Slater's ionic radius away from the average trend is due to the effects of the shell structure. Their role in determining the ionic radius can be most easily visualized based on the expression for the radius of the maximum electron density (30) which correlates with the ionic radius. This result emphasizes the following main principles:

(i) As Z increases, all the n levels move down in energy which amounts to replacing n by its effective counterpart $n^* \leq n$. If the electrons are added to an outer shell, the effective nuclear charge Z^*e seen by each of them gradually increases. This is because the outer shell electrons are relatively inefficient in shielding the nuclear charge. As a result the ion slowly contracts.

(ii) As a new outer shell begins to fill, the effect of going into the higher shell outweighs the effect of lowering of an n level as Z increases to $Z+1$. This corresponds to an abrupt increase of the effective principal quantum number n^* . Moreover, the effective charge Z^*e seen by the outermost electron drops because now all remaining $Z-2$ electrons belong to inner shells thus efficiently screening the nuclear charge. These changes in n^* and Z^* cause a sharp increase of the ion size.

Slater's rules [42] add a quantitative aspect to these principles. In the following explanation of the variation of the ionic radius, Fig. 11, we are always speaking of the

positive singly-charged ions whose electronic configurations are taken from the NIST database [43].

In going from ${}^2\text{He}$ ($1s^1$), to ${}^3\text{Li}$ ($1s^2$) the ion size decreases. As one moves to ${}^4\text{Be}$ ($[\text{He}]2s^1$) the added electron enters the higher $2s$ shell, and the ionic radius sharply increases. Similar increases take place as one goes from every alkali to the following alkali earth ion. A related jump in ionic radius also occurs past every noble element ion, ${}^{29}\text{Cu}$ ($[\text{Ar}]3d^{10}$) \rightarrow ${}^{30}\text{Zn}$ ($[\text{Ar}]3d^{10}4s^1$), ${}^{47}\text{Ag}$ ($[\text{Kr}]4d^{10}$) \rightarrow ${}^{48}\text{Cd}$ ($[\text{Kr}]4d^{10}5s^1$), and ${}^{79}\text{Au}$ ($[\text{Xe}]4f^{14}5d^{10}$) \rightarrow ${}^{80}\text{Hg}$ ($[\text{Xe}]4f^{14}5d^{10}6s^1$) because a higher s -shell starts to be occupied. An analogous argument explains the sharp increase of ionic radius while going from ${}^{24}\text{Cr}$ ($[\text{Ar}]3d^5$) to ${}^{25}\text{Mn}$ ($[\text{Ar}]3d^54s^1$) and from ${}^{42}\text{Mo}$ ($[\text{Kr}]4d^5$) to ${}^{43}\text{Tc}$ ($[\text{Kr}]4d^55s^1$)

As one moves from ${}^4\text{Be}$ ($[\text{He}]2s^1$) to ${}^{11}\text{Na}$ ($[\text{He}]2s^22p^6$) the $2s$ and $2p$ shells are filled by the electrons, and the ion size gradually decreases. A similar effect explains the decrease of the ionic radius along the ${}^{12}\text{Mg}$ ($[\text{Ne}]3s^1$)– ${}^{19}\text{K}$ ($[\text{Ne}]3s^23p^6$), ${}^{30}\text{Zn}$ ($[\text{Ar}]3d^{10}4s^1$)– ${}^{37}\text{Rb}$ ($[\text{Ar}]3d^{10}4s^24p^6$), ${}^{48}\text{Cd}$ ($[\text{Kr}]4d^{10}5s^1$)– ${}^{55}\text{Cs}$ ($[\text{Kr}]4d^{10}5s^25p^6$), and ${}^{80}\text{Hg}$ ($[\text{Xe}]4f^{14}5d^{10}6s^1$)– ${}^{87}\text{Fr}$ ($[\text{Xe}]4f^{14}5d^{10}6s^26p^6$) sequences.

The ionic radius decreases through the ${}^{20}\text{Ca}$ ($[\text{Ar}]4s^1$)– ${}^{21}\text{Sc}$ ($[\text{Ar}]3d^14s^1$)– ${}^{22}\text{Ti}$ ($[\text{Ar}]3d^24s^1$) segment. This happens because the electrons filling the $3d$ shell only partially screen the nuclear charge - as a result the outer $4s$ electron sees a gradual increase of effective Z^* . The same argument explains the decrease of ion size while going from ${}^{25}\text{Mn}$ ($[\text{Ar}]3d^54s^1$) to ${}^{26}\text{Fe}$ ($[\text{Ar}]3d^64s^1$) which is merely a continuation of the Ca-Ti segment. The decrease of ionic radius through the ${}^{73}\text{Ta}$ ($[\text{Xe}]4f^{14}5d^36s^1$)– ${}^{77}\text{Ir}$ ($[\text{Xe}]4f^{14}5d^76s^1$) series can be similarly understood. In fact, the first entry of this series is ${}^{70}\text{Yb}$ ($[\text{Xe}]4f^{14}5d^06s^1$) where we intentionally modified the standard notation to show the absence of the $5d$ electron.

The size of the ion first abruptly decreases while going from ${}^{22}\text{Ti}$ ($[\text{Ar}]3d^24s^1$) to ${}^{23}\text{V}$ ($[\text{Ar}]3d^4$) and then continues decreasing more gradually as one moves to ${}^{24}\text{Cr}$ ($[\text{Ar}]3d^5$). The sudden change is due to the fact that the outer shell changes from $4s$ to $3d$ which can be viewed as a decrease in the effective quantum number n^* . The subsequent slower increase of the ionic radius is due to the increase of the effective nuclear charge Z^*e seen by the larger number of $3d$ electrons. The same trend is exhibited in the ${}^{40}\text{Zr}$ ($[\text{Kr}]4d^25s^1$)– ${}^{41}\text{Nb}$ ($[\text{Kr}]4d^4$)– ${}^{42}\text{Mo}$ ($[\text{Kr}]4d^5$) sequence. A very similar behavior is found in the ${}^{26}\text{Fe}$ ($[\text{Ar}]3d^64s^1$)– ${}^{27}\text{Co}$ ($[\text{Ar}]3d^8$)– ${}^{28}\text{Ni}$ ($[\text{Ar}]3d^9$)– ${}^{29}\text{Cu}$ ($[\text{Ar}]3d^{10}$), ${}^{43}\text{Tc}$ ($[\text{Kr}]4d^55s^1$)– ${}^{44}\text{Ru}$ ($[\text{Kr}]4d^7$)– ${}^{45}\text{Rh}$ ($[\text{Kr}]4d^8$)– ${}^{46}\text{Pd}$ ($[\text{Kr}]4d^9$)– ${}^{47}\text{Ag}$ ($[\text{Kr}]4d^{10}$), and ${}^{77}\text{Ir}$ ($[\text{Xe}]4f^{14}5d^76s^1$)– ${}^{78}\text{Pt}$ ($[\text{Xe}]4f^{14}5d^9$)– ${}^{79}\text{Au}$ ($[\text{Xe}]4f^{14}5d^{10}$) series.

Superficially, a similar steep decrease of the ion size is followed by more gradual decrease in the ${}^{70}\text{Yb}$ ($[\text{Xe}]4f^{14}6s^1$)– ${}^{71}\text{Lu}$ ($[\text{Xe}]4f^{14}6s^2$)– ${}^{72}\text{Hf}$ ($[\text{Xe}]4f^{14}5d^16s^2$) sequence. This behavior can be explained by noticing that in both steps the effective Z^* felt by a $6s$ electron increases; the increase during the

second step is smaller because inner shell d electrons are more efficient in screening the nuclear charge than s electrons.

While going from ${}^{38}\text{Sr}$ ($[\text{Kr}]5s^1$) to ${}^{39}\text{Y}$ ($[\text{Kr}]5s^2$) and to ${}^{40}\text{Zr}$ ($[\text{Kr}]4d^25s^1$) a decrease of ionic radius follows by an increase. This happens because the effective Z^* felt by an outer $5s$ electron first increases and then decreases. The increase of the size of the ion is somewhat smaller than the decrease because two $4d$ electrons in Zr only partially shield two extra units of the nuclear charge.

For the ${}^{63}\text{Eu}$ ($[\text{Xe}]4f^76s^1$)– ${}^{64}\text{Gd}$ ($[\text{Xe}]4f^75d^16s^1$)– ${}^{65}\text{Tb}$ ($[\text{Xe}]4f^96s^1$) sequence the ionic radius first decreases and then increases back to its initial value. This happens because the d electron in Gd is less effective in shielding the nuclear charge than the f electron in Tb (considered perfect in Slater's scheme).

One of the less intuitive increases of ionic radius takes place while going from ${}^{56}\text{Ba}$ ($[\text{Xe}]6s^1$) to ${}^{57}\text{La}$ ($[\text{Xe}]5d^2$). On one hand, the effective principal quantum number n^* decreases which according to (30) should lower the ionic radius. However as compared to the $6s$ electron of Ba, the effective Z^* seen by one of La's $5d$ electrons also decreases. This happens because the inner shell $5sp$ electrons screen the nuclear charge more effectively if the outer shell electrons are in a d state (La) as compared to an s state (Ba). As a result the decrease in Z^* outweighs the decrease in n^* thus leading to an increase of the ion size. A very similar argument explains the reversed decrease of ionic radius taking place as one goes from ${}^{58}\text{Ce}$ ($[\text{Xe}]4f^15d^2$) (whose size is identical to that of La) to ${}^{59}\text{Pr}$ ($[\text{Xe}]4f^36s^1$) (identical in size to Ba). Here the role of the $4f$ electrons merely reduces to compensating for the increase of the nuclear charge.

The ionic radius does not change as one moves from ${}^{57}\text{La}$ ($[\text{Xe}]5d^2$) to ${}^{58}\text{Ce}$ ($[\text{Xe}]4f^15d^2$) because the increase of nuclear charge is exactly compensated by adding a $4f$ electron. The same argument explains the constancy of the ionic radius along most of the lanthanide sequence, ${}^{59}\text{Pr}$ ($[\text{Xe}]4f^36s^1$)– ${}^{63}\text{Eu}$ ($[\text{Xe}]4f^76s^1$), ${}^{65}\text{Tb}$ ($[\text{Xe}]4f^96s^1$)– ${}^{70}\text{Yb}$ ($[\text{Xe}]4f^{14}6s^1$). The only exception from this trend, ${}^{64}\text{Gd}$ ($[\text{Xe}]4f^75d^16s^1$), has already been discussed.

Now when the variations of the Slater's ionic radius are understood, we can compare them with experimental and numerical modulations of the quantum defect. Since the numerical data are more extensive than experimental findings, and the agreement between the two is fairly good, in Fig. 11 we only show the variation of the numerically evaluated quantum defect $\delta\mu = \mu - \mu_{sc}$. The inspection of Fig. 11 leaves no doubt that the variations of the quantum defect with $Z^{1/3}$ are correlated with those of the Slater's ionic radius - even the minute changes of the latter find their way in the corresponding changes of the former.

There are however two places where it appears there is a disagreement with expectation:

(i) Along most of the lanthanide sequence the Slater's ionic radius does not change while the variation of the

quantum defect decreases. This can be understood as an artifact of the Slater's rules. In reality the f electrons do not perfectly screen the nuclear charge. Therefore the effective charge seen by the outer $6s$ electron increases with $Z^{1/3}$ and correspondingly the ionic radius should decrease. Then the quantum defect variation should decrease as well which is in correspondence with numerical results. We also note that the Gd dip of the ionic radius is reproduced in the quantum defect variation.

(ii) For the elements past Hg, the Slater's ionic radius decreases with $Z^{1/3}$ while the variation of the quantum defect increases. The reason why it happens is unclear. It cannot be ruled out that here the effects of the shell structure might be so strong that our correlation rule derived from semiclassical arguments breaks down qualitatively.

Overall, the analysis of this section makes it certain that the gross features of the quantum defect variation with $Z^{1/3}$ are due to the effects of the shell structure.

B. Zel'dovich modulation

Qualitative analysis is of little use in trying to see the Zel'dovich effect in experimental and numerical data because the Zel'dovich modulation has an amplitude which is several times smaller than that due to the effects of the shell structure (see Fig. 10). A way to proceed quantitatively is suggested by the fashion in which the shell and systematic effects are coupled.

Inspecting the limiting expression for the Zel'dovich modulation, Eq. (24), it is straightforward to see that after replacing systematic $U_s(r)$ with the one accounting for the shell structure, the amplitude of the Zel'dovich modulation will become strongly sensitive to the effects of the shell structure because it is determined by the logarithmic derivative of the inner potential $U_s(r)$ and the range parameter x_0 . On the other hand, the period of the oscillation is far less sensitive to the effects of the shell structure since it is determined by the number of de Broglie's half-waves fitting inside the ionic core of the atom.

This last observation suggests that it might be possible to see the Zel'dovich effect in the experimental and numerical Fourier spectra of the quantum defect variation $\delta\mu = \mu - \mu_{sc}$ (see Fig. 10) as a peak whose location can be brought in correspondence with the systematic theory. To proceed in this direction, in a range of $Z^{1/3}$ of length L we expand the quantum defect variation into a Fourier series

$$\delta\mu(Z^{1/3}) = \sum_{k=2\pi p/L} \mu_k \exp(ikZ^{1/3}) \quad (31)$$

where $p = 0, \pm 1, \pm 2, \dots$. In order to numerically evaluate the Fourier coefficients $\mu_k = \mu_{-k}^*$, the experimental and numerical $\delta\mu(Z^{1/3})$ dependences (see Fig. 10) were fitted with a cubic spline which was then sampled equidistantly

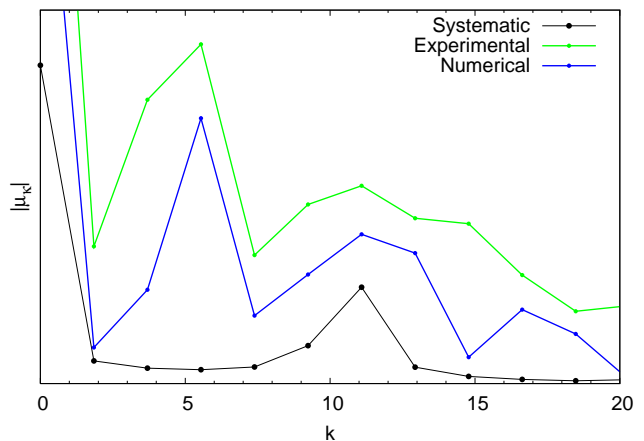


Figure 12: Systematic, experimental and numerical amplitudes of the Fourier coefficients of the quantum defect variation (arbitrary units, same normalization) $|\mu_k|$ as functions of k for $k \geq 0$. The peaks at $k \simeq 11$ correspond to the Zel'dovich effect.

in $Z^{1/3}$ to extract the Fourier spectrum. The result for the magnitude of the Fourier coefficients $|\mu_k|$ as a function of k is displayed in Fig. 12 as a series of solid dots which for convenience are connected by straight line segments. The uncertainty of the location of each dot along the k axis, $2\pi/L$, is the distance between the nearest values of k . Since the last available experimental quantum defect corresponds to ^{83}Bi (see Table 1), for both experimental and numerical data we restricted ourselves to $L = 83^{1/3}$. The finite values of μ_0 correspond to the presence of nonzero background in experimental and numerical $\delta\mu(Z^{1/3})$ dependences and are of no interest to us.

For comparison in Fig. 12 we also show the Fourier spectrum of our systematic calculation which, as expected, has only one peak corresponding to the Zel'dovich effect. The position of the peak along the k axis can be understood from the large Z asymptotics of the Thomas-Fermi action $S_0/\hbar \simeq 5.2Z^{1/3}$ (28). Comparing this with the limiting expression for the Zel'dovich modulation (24) we would expect a peak at $k \simeq 10.4$. The peak in Fig. 12 is located at a slightly different value of $k \simeq 11$ which is due to the fact that the asymptotic behavior $S_0/\hbar \simeq 5.2Z^{1/3}$ becomes numerically accurate only for $Z^{1/3}$ exceeding 10.

Both the experimental and numerical spectra in Fig. 12 have peaks at the same value of $k \simeq 11$ which we argue are the signatures of the Zel'dovich effect.

It is curious that both experimental and numerical spectra have another peak in common located at $k \simeq 5.5$. This peak which is about twice as high as that due to the Zel'dovich effect is natural to relate to the effects of the shell structure. The existence of this peak translates into the $(2\pi/5.5)Z^{1/3} = 1.14Z^{1/3}$ periodicity of the quantum defect variation due to the effects of the shell structure. This conclusion resembles the $Z^{1/3}$ periodic oscillation of

the ground-state energy of an atom away from the systematic trend [45]. With uncertainty of the peak location in mind, one may speculate that our result is a manifestation of the same effect for highly-excited states. More work is necessary to bring understanding to this issue.

We also repeated the same Fourier analysis by choosing the range of $Z^{1/3}$ to be $L = 102^{1/3}$ which includes all the numerical data. As far as experimental data go in the range of $Z^{1/3}$ between $83^{1/3}$ and $102^{1/3}$ we used extrapolation of our cubic spline fit. As a result the peaks just discussed slightly change their positions and amplitudes but within the $2\pi/L$ uncertainty systematic, experimental and numerical Fourier spectra share a peak in common corresponding to the Zel'dovich effect. Similarly, experimental and numerical spectra continue to share a peak in common due to the effects of the shell structure.

V. CONCLUSIONS AND FUTURE DIRECTIONS

In this paper we analyzed in a model-independent fashion the weakly-bound s spectra of the distorted Coulomb problem for arbitrary relationship between the range of the inner potential and Bohr's radius of the Coulomb field. We demonstrated that the spectra are fairly sensitive to the binding properties of the inner potential which constitutes the essence of the Zel'dovich effect, and established the corresponding details of spectral changes. Armed with these results, we conducted an analysis of experimental and numerical Rydberg spectra of atoms along the Periodic Table which indeed show an evidence of the Zel'dovich effect. Our analysis can be extended and adopted in several directions:

First, there is an abundance of experimental and numerical data for atomic Rydberg states of finite angular

momenta which are likely to contain signatures of the Zel'dovich effect. However, in the limit of a very short-ranged inner potential the way the effect manifests itself is somewhat different from its s state counterpart [7]. This observation makes it pertinent to generalize our analysis to the case of finite angular momentum.

It has been known for some time [46] that the Rydberg formula (2) is superior to the Wannier (Bohr) formula quoted in textbooks [2] in representing excitonic spectra in condensed matter systems. Experimental examples here include clean and doped rare-gas solids and rare-gas impurities in solid hydrogen. Although this is a context in which the Zel'dovich effect has been originally discovered [3], to the best of our knowledge there were no attempts to relate it to excitonic quantum defects. Because of the dielectric screening of the Coulomb interaction, the Zel'dovich effect in these systems is expected to be more pronounced than in atomic Rydberg spectra. Only minor changes to our analysis are needed to understand the excitonic Rydberg spectra.

Other examples of systems where the Zel'dovich effect should have experimental signatures include Rydberg ions and electronic image states [47].

VI. ACKNOWLEDGMENTS

We are grateful to T. F. Gallagher and R. R. Jones for sharing with us their expertise. We also acknowledge R. M. Kalas and X. Yang who participated in the initial stages of this project. This work was supported by the Chemical Sciences, Geosciences and Biosciences Division, Office of Basic Energy Sciences, Office of Science, U. S. Department of Energy.

-
- [1] L. D. Landau and E. M. Lifshitz, *Quantum Mechanics*, (Pergamon, New York, 1977), Sections 117 and 138.
- [2] N. W. Ashcroft and N. D. Mermin, *Solid State Physics*, (Saunders, Philadelphia, 1976), Chapter 30.
- [3] Ya. B. Zel'dovich, *Fiz. Tverd. Tela* (Leningrad), **1**, 1637 (1959) [*Sov. Phys. Solid State* **1**, 1497 (1959)].
- [4] Sections 21 and 32 of Ref. [1].
- [5] V. S. Popov, *Zh. Eksp. Teor. Fiz.* **60**, 1228 (1971) [*Sov. Phys. JETP* **33**, 665 (1971)].
- [6] A. E. Kudryavtsev, V. E. Markushin, and I. S. Shapiro, *Zh. Eksp. Teor. Fiz.* **74**, 432 (1978) [*Sov. Phys. JETP* **47**, 225 (1978)]; I. S. Shapiro, *Phys. Rep.* **35C**, 131 (1978)]; D. A. Kirzhnits and F. M. Pen'kov, *Zh. Eksp. Teor. Fiz.* **82**, 657 (1982) [*Sov. Phys. JETP* **55**, 393 (1982)].
- [7] A. E. Kudryavtsev and V. S. Popov, *Pis'ma Zh. Eksp. Teor. Fiz.* **29**, 311 (1979) [*Sov. Phys. JETP Lett.* **29**, 280 (1979)], V. S. Popov, A. E. Kudryavtsev and V. D. Mur, *Zh. Eksp. Teor. Fiz.* **77**, 1727 (1979) [*Sov. Phys. JETP* **50**, 865 (1979)], V. S. Popov, A. E. Kudryavtsev, V. I. Lisin, and v. D. Mur, *Zh. Eksp. Teor. Fiz.* **80**, 1271 (1981) [*Sov. Phys. JETP* **53**, 650 (1981)], B. M. Karnakov, A. E. Kudryavtsev, V. D. Mur, and V. S. Popov, *Zh. Eksp. Teor. Fiz.* **94**, 65 (1988) [*Sov. Phys. JETP* **68**, 1333 (1988)].
- [8] B. M. Karnakov, *Pis'ma Zh. Eksp. Teor. Fiz.* **77**, 73 (2003) [*JETP Lett.* **77**, 68 (2003)], V. S. Popov, *ibid.* **79** (2003) [*ibid.* **74** (2003)].
- [9] H. Friedrich, *Theoretical Atomic Physics*, (Springer-Verlag, 1991).
- [10] R. Latter, *Phys. Rev.* **99**, 510 (1955).
- [11] S. T. Manson, *Phys. Rev.* **182**, 97 (1969).
- [12] U. Fano, C. E. Theodosiou and J. L. Dehmer, *Rev. Mod. Phys.* **48**, 49 (1976).
- [13] F. Herman and S. Skillman, *Atomic Structure Calculations* (Prentice-Hall, Englewood Cliffs, N. J., 1963).
- [14] A. B. Migdal, *Qualitative Methods in Quantum Theory* (Benjamin, Reading, MA, 1977), Chapter 3.
- [15] N. N. Lebedev, *Special Functions and Their Applications*, (Prentice-Hall, Inc. Englewood Cliffs, New Jersey, 1965).
- [16] L. D. Landau and Ya. A. Smorodinskii, *Zh. Eksp. Teor.*

- Fiz. **14**, 269 (1944); see also Eq. (138.12) of Ref. [1].
- [17] S. Deser, M. L. Goldberger, K. Baumann, and W. Thirring, Phys. Rev. **96**, 774 (1954).
- [18] A more accurate calculation based on Eq.(11) gives $\mu = -2a_s/a_B - x_0^4/32$ which is negative for sufficiently weak $U_s(r)$; for $x_0 \ll 1$ this effect however is negligible as can be seen from Fig. 3.
- [19] Section 132 of Ref. [1].
- [20] Section 133 of Ref. [1].
- [21] A generalization of Levinson's theorem to potentials with Coulomb tails can be found in Z. R. Iwinski, L. Rosenberg, and L. Spruch, Phys. Rev. Lett. **54**, 1602 (1985), and Z. Ma Phys. Rev. D **33**, 1745 (1986).
- [22] M. V. Berry, Sci. Prog., Oxf. **57**, 43 (1969).
- [23] M. V. Berry and K. E. Mount, Rep. Prog. Phys. **35**, 315 (1972).
- [24] Section 70 of Ref. [1].
- [25] Eq.(24) predicts that there is an unphysical divergence as $Z \rightarrow 1 + 0$ which is present but hardly noticeable in the inset. The oscillation shown in bold is everywhere finite.
- [26] L. B. Robinson, Phys. Rev. **117**, 1281 (1960).
- [27] A. A. Radzig and B. M. Smirnov, *Reference Data on Atoms, Molecules and Ions*, (Springer-Verlag, 1985), Table 5.2, and references therein.
- [28] C. Jaffé and W. P. Reinhardt, J. Chem. Phys. **66**, 1285 (1977), and references therein.
- [29] TOPbase: on-line interactive database of atomic data, <http://vizier.u-strasbg.fr/topbase/home.html>.
- [30] K. Radler and J. Berkowitz, J. Chem. Phys. **70**, 216 (1979).
- [31] S. F. Dyubko, V. A. Efremov, V. G. Gerasimov and K. B. MacAdam, J. Phys. B: At. Mol. Opt. Phys. **37**, 1967 (2004).
- [32] B. Ruscic and J. Berkowitz, Phys. Rev. A **40**, 6716 (1989).
- [33] R. H. Page and C. S. Gudeman, J. Opt. Soc. Am. B **7**, 1761 (1990).
- [34] M. Kompitsas, C. Baharis, and Z. Pan, J. Opt. Soc. Am. B **11**, 697 (1994).
- [35] W. Li, I. Mourachko, M. W. Noel and T. F. Gallagher, Phys. Rev. A **67**, 052502 (2003).
- [36] Z. J. Jakubek and B. Simard, J. Phys. B: At. Mol. Phys. **33**, 1827 (2000).
- [37] D. M. Rayner, S. A. Mitchell, O. L. Bourne and P. A. Hackett, J. Opt. Soc. Am. B **4**, 900 (1987).
- [38] F. Federmann, K. Hoffmann, N. Quaas, and J.D.Close, Phys. Rev. Lett. **83**, 2548 (1999).
- [39] J. H. M. Neijzen and A Dönszelmann, J. Phys. B: At. Mol. Phys. **15**, 1981 (1982).
- [40] P. Goy, J. M. Raimond, G. Vitrant and S. Haroche, Phys Rev A **26**, 2733 (1982).
- [41] G. J. Ding, R. C. Shang, L. F. Chang, K. L. Wen, Q. Hui, and D. Y. Chen, J. Phys. B: At. Mol. Opt. Phys. **22**, 1555 (1989).
- [42] J. C. Slater, Phys. Rev. **36**, 57 (1930).
- [43] *Atomic Reference Data for Electronic Structure Calculations*, <http://physics.nist.gov/PhysRefData/DFTdata/>.
- [44] *CRC Handbook of Chemistry and Physics*, D. R. Lide, Editor-in-Chief, 84th Edition 2004-2005 (Boca Raton, CRC Press, LLC), **12-14**; <http://www.hbcnetbase.com/>. The crystal ionic radius of the same ion varies with its coordination number; the data shown in Fig. 11 are averages (if more than one coordination number is possible).
- [45] B.-G. Englert, *Semiclassical Theory of Atoms*, Lecture Notes in Physics, 300 (Springer-Verlag, Berlin, 1988), Chapter 5, and references therein.
- [46] L. Resca and R. Resta, Phys. Rev. B **19**, 1683 (1979), and references therein; V. Saile, R. Reininger, P. Laporte, I. T. Steinberg, and G. L. Findley, Phys. Rev. B **37**, 10901 (1988), and references therein.
- [47] S. G. Davison and M. Stes'licka, *Basic Theory of Surface States*, (Clarendon Press, Oxford, 1992), Chapter 7, and references therein.